Protein Resistance of Surfaces Prepared by Chemisorption of Monothiolated Poly(ethylene glycol) to Gold and Dendronization with Aliphatic Polyester Dendrons: Effect of Hydrophilic Dendrons

S. Rahima Benhabbour,[†] Lina Liu,[‡] Heather Sheardown,[‡] and Alex Adronov*,[†]

Department of Chemistry and the Brockhouse Institute for Materials Research and Department of Chemical Engineering, McMaster University, Hamilton, Ontario L8S 4M1, Canada

Received September 14, 2007; Revised Manuscript Received December 18, 2007

ABSTRACT: Protein adsorption to surfaces prepared by chemisorption of thiol-terminated poly(ethylene glycol) (HS-PEG_{650}-OH) to gold-coated silicon wafers followed by functionalization of the terminal PEG OH groups with aliphatic polyester dendrons was investigated. Chemisorption of HS-PEG_{650}-OH to the gold surfaces was carried out under cloud-point conditions to give a chain density of ∼3.7 chains/nm^2, as calculated from AFM film thickness measurements. Dendronization of the PEG-functionalized surfaces with aliphatic polyester dendrons, generations 1−4, was achieved using divergent dendron growth. The hydrophilicity of the surfaces increased significantly with increasing dendron generation as shown by water contact angle data. The effect of the hydrophilic dendrons on protein adsorption from phosphate-buffered saline (PBS) and plasma are reported. Adsorption of both ^{125}I-radiolabled fibrinogen and lysozyme onto the dendronized surfaces showed that protein adsorption increases upon introduction of dendrons to the PEG-functionalized surfaces. The similarity between fibrinogen and lysozyme adsorption suggests that resistance of the dendronized surfaces to proteins follows the same trend regardless of protein size.

Introduction

Among the biomaterials under investigation, polymers constitute a versatile class that has received attention in various biological applications due to the vast flexibility in their synthesis and facile modification to suit specific physical and mechanical properties of a wide range of tissues. In comparison to natural polymers, the use of synthetic polymers as biomaterials is a relatively recent phenomenon.[1] A variety of polymers, including polyurethanes, polyethylene, poly(ethylene terephthalate), silicones, and various polyacrylates, have been used in applications such as blood contacting devices, hip joint replacement, and intraocular lenses.[1] Even though the application of biostable polymeric materials has played an important role in the advancement of modern health care, many of these materials are limited by their lack of long-term biocompatibility.

Protein adsorption is known to be the first event that occurs following implantation of biomaterials and is therefore important in initiating events that determine host responses such as blood coagulation, thrombus formation, platelet activation, bacterial infection, and other undesirable responses.[2,3] Surfaces that resist the nonspecific protein adsorption are useful in numerous applications, including sensors, materials for contact lenses, implantable devices in blood contacting applications,[2] and drug delivery devices.[4] A common approach for minimizing problems arising from protein adsorption involves coating the surface with a material that inhibits nonspecific interactions. A number of such materials have been used, including heparin,[5] dextran,[6] and poly(ethyloxazoline).[7,8] However, the most prominent and commonly used material for protein adsorption resistance is poly(ethylene glycol) (PEG).[9] While a number of different PEG-functionalized surfaces have been studied,[10–15] a molecular-level understanding of their protein-repelling mechanisms is still a matter of debate.[16–18] For example, Nishiumi and co-workers suggested that protein resistance of the PEG-modified surfaces is directly attributed to the highly dynamic nature of the segments in water.[19] On the basis of a model study by Andrade and de Gennes to rationalize the protein resistance of surfaces grafted with PEG, it was found that the conformational flexibility of the grafted PEG plays an important role in this process.[14,15,20] In separate studies, Grunze and co-workers[17,21] found that the conformation of PEG chains at the interface and their interaction with water is an important determinant of protein resistance, whereas Brash and co-workers have reported that chain density is one of the key contributors to this phenomenon.[3,12,22,23]

While these studies have thoroughly investigated the protein-resistant properties of linear hydrophilic polymers, focusing on hydrophilicity/hydration, conformation, molecular weight, and surface density, relatively little attention has been given to the effect of polymer branching on protein repulsion. Although branched polymers and dendrimers have attracted significant interest as drug delivery vehicles,[24–27] investigation of their antifouling properties on surfaces has been limited to the use of PAMAM dendrimers and polyglycerol hyperbranched polymers.[28–30] In the case of PAMAM dendrimers, protein resistance was significantly diminished as a result of their polycationic nature under physiological pH.[31,32] Nonspecific protein adsorption is known to be exacerbated on cationic surfaces relative to neutral surfaces.[33] Hyperbranched polyglycerols, on the other hand, are neutral under physiological conditions. These structures were shown to exhibit protein resistance that is practically equivalent to a PEG monolayer on gold.[30] However, the polymerization mechanism precludes precise control of polymer size, architecture, and degree of branching in these materials. Here, we present the synthesis and characterization of model dendronized gold surfaces, which combine the linear PEG with aliphatic polyester dendrons based on the 2,2-bis(hydroxymethyl)propionic acid (bis-MPA) building block. Similar to the hyperbranched polyglycerols, the polyester dendrons exhibit charge neutrality under physiological conditions and a well-defined structure that arises from their stepwise synthesis. In addition, the dendrons investigated here have been shown to be biocompatible, making them ideal for biological applica-

* Corresponding author: Tel (905) 525-9140 x23514; Fax (905) 521-2773; e-mail adronov@mcmaster.ca.
[†] Department of Chemistry and the Brockhouse Institute for Materials Research.
[‡] Department of Chemical Engineering.

10.1021/ma702074v CCC: $40.75
Published on Web 02/28/2008

tions.[34,35] The focus of this study was therefore to investigate the effect of surface functionalization with hydrophilic bis-MPA-based polyester dendrons on protein adsorption at each dendrimer generation and to compare this system with more traditional PEG-grafted surfaces.

Experimental Section

General. DOWEX50W-X2 ion-exchange resin, 4-(dimethylamino)pyridine (DMAP) (99%), 2,2-bis(hydroxymethyl)propionic acid (bisMPA), 2,2-dimethoxypropane, *p*-toluenesulfonic acid monohydrate (TsOH), and *N,N′*-dicyclohexylcarbodiimide (DCC) were purchased from Aldrich. Thiol-terminated poly(ethylene glycol) (HS-PEG_{650}-OH) was purchased from Polymer Source, Inc. Dichloromethane (CH_2Cl_2), ethyl acetate (EtOAc), and hexanes were purchased from CALEDON. Acetonide protected anhydride of bis-MPA (**1**) was prepared according to literature procedures.[36] All reagents were used as received.

Gold substrates prepared by electron beam evaporation of silicon wafers with an adhesive titanium tungstate (TiW) layer (300 Å) followed by a layer of gold (1000 Å) were purchased from Thin Film Technology, Buellton, CA, and diced into 1.0 × 1.0 cm^2 pieces. Prior to chemisorption, the surfaces were cleaned, using a literature procedure by immersing them in chromosulfuric acid (H_2SO_4 >92%, CrO_3 >1.3%) for 1 h to remove any organic contaminants, followed by ultrasonication in both Milli-Q water and ethanol for 10 min and extensive rinsing with Milli-Q water.[24] Sessile-drop water contact angles were determined using water droplets with a 1–2 μL volume. Advancing and receding angles were obtained using a Ramé-Hart NRL 100-00 goniometer (Mountain Lakes, NJ). All dendronization reactions were carried out on a VWR S-500 orbital shaker since no stirring was possible.

X-ray photoelectron spectroscopy (XPS) data were obtained using a Leybold (Specs, Berlin) MAX 200 XPS system employing a nonmonochromated Al Kα source operating at 15 kV and 20 mA. Low-resolution spectra (pass energy = 192 eV) were used to determine atomic compositions; high-resolution C 1s spectra (pass energy = 48 eV) provided additional surface structural information. Specslab (Specs, Berlin) software was used for spectral fitting. Spectra were taken at two takeoff angles: 90° and 20° relative to the surface. The respective spot sizes were 4 × 7 and 1 × 1 mm; the smaller area at 20° was used to ensure that the beam footprint remained on the samples.

Time-of-flight secondary ion mass spectrometry (TOF-SIMS) measurements were obtained with an ION-TOF TOF-SIMS IV (ION-TOF GmbH, Germany) instrument using 25 keV Ga^+ primary ions (average current of 2.5 pA) in high current bunched mode. The data were acquired over a 500 × 500 μm^2 area, and low-energy electron flooding was used for charge compensation. The primary ion dose was kept below 10^{12} ions cm^{-2} to ensure static SIMS condition. The mass calibrations of the positive and negative ion spectra were performed internally using CH_3^+, $C_2H_3^+$, $C_2H_5^+$, and $C_5H_7^+$ peaks and C^-, CH^-, C_2H^-, C_3H^-, and C_4H^- peaks. A complementary approach of the hypothesized structure of the surface has been used to identify and assign specific fragments.

Atomic force microscopy (AFM) analyses were carried out using a Digital Instruments NanoScope IIIa Multimode AFM equipped with a vertical engage "E" scanner with 15 μm full range scan. The images were recorded with standard tips in tapping mode at a scan rate of 0.5 Hz.

Proteins. Fibrinogen was purchased from Calbiochem (La Jolla, CA), dialyzed against Tris buffer, pH 7.4, aliquoted, and stored at –70 °C. The molecular weight and dimensions of fibrinogen are 3.4×10^5 Da and 450 × 90 × 90 $Å^3$, respectively, and its isoelectric point is 5.5. Lysozyme was obtained from Calbiochem (La Jolla, CA) and used as received. The molecular weight and dimensions of lysozyme are 1.43×10^4 Da and 45 × 30 × 30 $Å^3$, respectively, and its isoelectric point is 11.0.

Chemisorption of Surfaces with HS-PEG_{650}-OH. After cleaning, the surfaces were immediately transferred to 24-well plates containing the chemisorption solution. This solution consisted of 5 mM of HS-PEG_{650}-OH in phosphate-buffered saline (PBS) at pH 7.4. The chemisorption was carried out for various time periods at 25 °C with two different ionic strengths (IS), adjusted using sodium chloride (NaCl), in order to optimize the conditions for surface chain density. Following chemisorption, the surfaces were transferred to vials containing Milli-Q water and ultrasonicated for 10 min. This was followed by ultrasonication in ethanol for 10 min and finally extensive rinsing with Milli-Q water (~20 mL). The surfaces were dried with a stream of nitrogen (N_2) prior to contact angle, XPS, and AFM analysis.

General Esterification Reaction: Preparation of Au-G1-(Ac) Surfaces. To flame-dried 15 mL vials under argon, each charged with a PEG_{650}-functionalized surface in a solution of CH_2Cl_2:pyridine (3:2 v/v, 3 mL), excess acetonide anhydride (**1**) (0.1 g, 3.03×10^{-4} mol) along with a catalytic amount of DMAP (10 mg, 8.18×10^{-5} mol) was added, and the vials were shaken for 24 h at room temperature using an orbital shaker since no stirring was possible. The surfaces were transferred to new individual vials containing CH_2Cl_2 (5 mL) and ultrasonicated for 10 min to remove the unreacted acetonide anhydride. This was followed by ultrasonication of the surfaces in Milli-Q water (~5 mL) for 10 min, extensive rinsing with Milli-Q water (~20 mL) and ethanol (~20 mL), and finally drying with a stream of N_2 prior to analysis. For subsequent dendronization steps, all reagent quantities remained the same except for the amount of acetonide (**1**), the amount of DMAP, and the reaction time, which were as follows: Au-G2(Ac): 0.12 g of **1**, 12 mg of DMAP, 36 h; Au-G3(Ac): 0.15 g of **1**, 15 mg of DMAP, 48 h; Au-G4(Ac): 0.2 g of **1**, 20 mg of DMAP, 72 h.

General Deprotection Reaction: Preparation of Au-G1-(OH) Surfaces. The G1(Ac)-functionalized surfaces were individually placed in 5 mL vials charged with methanol (5 mL). To these vials was added the acidic resin DOWEX 50W-X2 (~0.50 g) such that complete coverage of the grafted surfaces was achieved. The vials were transferred to an oil bath at 50 °C and incubated for 1 h. The surfaces were transferred to new vials charged with methanol (5 mL) and ultrasonicated for 10 min. This step was followed by extensive rinsing with methanol (~20 mL) and immersion in methanol overnight. The surfaces were then dried with a stream of N_2 prior to the next esterification reaction. Deprotection of higher generation dendronized surfaces was done identically to the above.

AFM Analysis. The AFM analyses were carried out using the "scratch" method, where a scratch was introduced on a clean gold surface prior to functionalization. To ensure that the scratch penetrated the entire gold layer, scratch thickness was measured by AFM at numerous points along the scratch and compared to the known gold layer thickness from the manufacturer (100 nm). If the "trench" produced by scratching the surface was equal to or greater than 100 nm, the surface was used for subsequent experiments. On one side, across the scratch, the gold surface was coated with a temporary layer of poly(styrene) (PS) to prevent chemisorption of HS-PEG_{650}-OH, leaving this half unfunctionalized. After chemisorption on the exposed side, the surface was rinsed extensively with THF (~50 mL) to remove the PS film. The partially functionalized surface was ultrasonicated for 10 min in both Milli-Q water and ethanol and dried with N_2 prior to AFM analysis. AFM step-height measurements were carried out at multiple points (15 × 15 μm^2) of both unfunctionalized and PEG-grafted parts of the surface. Using the average mode in the AFM Nanoscope-(R) III Digital Instruments-version 5.30 program at each image collected, the PEG film thickness was calculated as the difference in average height between the two parts of the surface. Similar height measurements were carried out on the same surface after esterification of PEG-OH to introduce the first generation protected dendrons and at each step of dendronization up to the fourth generation.

Protein Adsorption. Fibrinogen and lysozyme (Calbiochem, La Jolla, CA) were radiolabeled with $Na^{125}I$ (ICN, Irvine, CA) using the iodine monochloride method and passed through a column

Table 1. Water Contact Angles (deg) under Various Chemisorption Conditions: Effect of Ionic Strength and Time on Surface Grafting Density

chemisorption conditions[a]	advancing contact angle (deg)	receding contact angle (deg)	ionic strength (M)
bare Au	70 ± 3	40 ± 8	
high IS (low solubility), 30 min	45 ± 2	15 ± 5	2.9
high IS, 2 h	41 ± 3	17 ± 4	2.9
high IS, 4 h	38 ± 2	15 ± 6	2.9
high IS, 12 h	36 ± 1	15 ± 3	2.9
low IS (high solubility), 30 min	58 ± 4	25 ± 3	0.26
low IS, 2 h	55 ± 3	26 ± 1	0.26
low IS, 4 h	47 ± 2	28 ± 2	0.26
low IS, 12 h	46 ± 3	27 ± 4	0.26

[a] 5 mM chemisorption solution of HS-PEG$_{650}$-OH in PBS at pH = 7.4.

packed with AG 1-X4 resin (Bio-Rad Laboratories, Inc.) in Tris buffer saline (TBS, pH 7.4) to remove unbound ^{125}I (held to <1% of total solution radioactivity). Prior to protein adsorption experiments, gold-coated silicon wafers were equilibrated in PBS-NaI buffer overnight; "cold" NaI was added to the buffer to prevent uptake of unbound ^{125}I to the gold.[37] Protein adsorption experiments were performed in PBS-NaI buffer (pH 7.4) at a protein concentration of 1 mg/mL (10% labeled, 90% "cold"/PBS and 2.5% labeled, 97.5% "cold"/plasma). The surfaces were placed in the wells of 24-well plates and incubated in a 1 mL solution of ^{125}I-labeled protein in PBS-NaI for 3 h at room temperature (22 °C). It was determined that no further adsorption occurred at times longer than 3 h.[3] The surfaces were rinsed three times (10 min each) with fresh PBS-NaI to remove any loosely bound protein. Surface radioactivity was determined, using a Perkin-Elmer WIZARD 3″ 1480 automatic gamma counter. The percent reduction of adsorption on the PEO-functionalized and dendronized surfaces relative to the unmodified gold was determined.

Results and Discussion

Surface Grafting with HS-PEG$_{650}$-OH. Surface dendronization was preceded by the chemisorption of monothiolated PEG, HS-PEG$_{650}$-OH, onto the gold surfaces. Conditions for the chemisorption of HS-PEG$_{650}$-OH were optimized by varying the ionic strength of the chemisorption solution as well as the chemisorption time at 25 °C. This strategy was based on the previously reported premise that higher chain densities should be obtained when chemisorption is carried out under cloud-point conditions.[38] The surface grafting was evaluated by water contact angle measurements. On the basis of the results from advancing contact angle measurements, higher chain densities were obtained in the high ionic strength (IS = 2.9, pH = 7.4) chemisorption solution after 4 h or longer at 25 °C, as reflected by the decrease in the contact angle (Table 1). On the basis of these results, all subsequent chemisorptions were carried out using a solution of 5 mM of HS-PEG$_{650}$-OH in high IS PBS for 4 h at 25 °C.

Divergent Dendron Synthesis. Growth of aliphatic polyester dendrons up to the fourth generation was accomplished using a divergent synthetic approach[39] with the acetonide-protected anhydride of 2,2-bis(hydroxylmethyl)propionic acid (bis-MPA) (**1**) as the building block (Scheme 1). The reactivity of this anhydride has proven to be useful for the synthesis of dendrimers,[36,40–43] dendronized polymers,[25,44–50] and dendronized surfaces.[24,51–53] The first generation dendrons were introduced via an esterification reaction carried out on the terminal hydroxyl groups of PEG$_{650}$-functionalized gold surfaces with excess acetonide anhydride (**1**) and a catalytic amount of DMAP in a mixture of CH_2Cl_2:pyridine (3:2 v/v). This step was followed by removal of the acetonide protecting groups to give the hydroxyl-terminated first generation dendrons. The deprotection step was carried out following a literature procedure, using the acidic resin DOWEX 50W-X2 in methanol at 50 °C for 1 h.[24] Iterative esterification and deprotection reactions allowed surface dendronization up to the fourth generation (Scheme 1).

Water Contact Angle Measurements. Water contact angles were measured before and after surface grafting with PEG and further dendronization with the aliphatic polyester dendrons of generation 1–4. It is apparent from the results (Table 1, Figure 1) that the surfaces grafted with HS-PEG$_{650}$-OH show a significant decrease in contact angle when compared to the unmodified gold surfaces. The advancing and receding angles on unmodified gold were 70 ± 3° and 40 ± 8°, respectively. Following chemisorption with PEG, the angles decreased significantly for all chemisorption conditions, reflecting the hydrophilic nature imparted by the grafted PEG on the gold surfaces (Table 1).

Scheme 1. Synthesis of G1−G4 Dendronized Surfaces

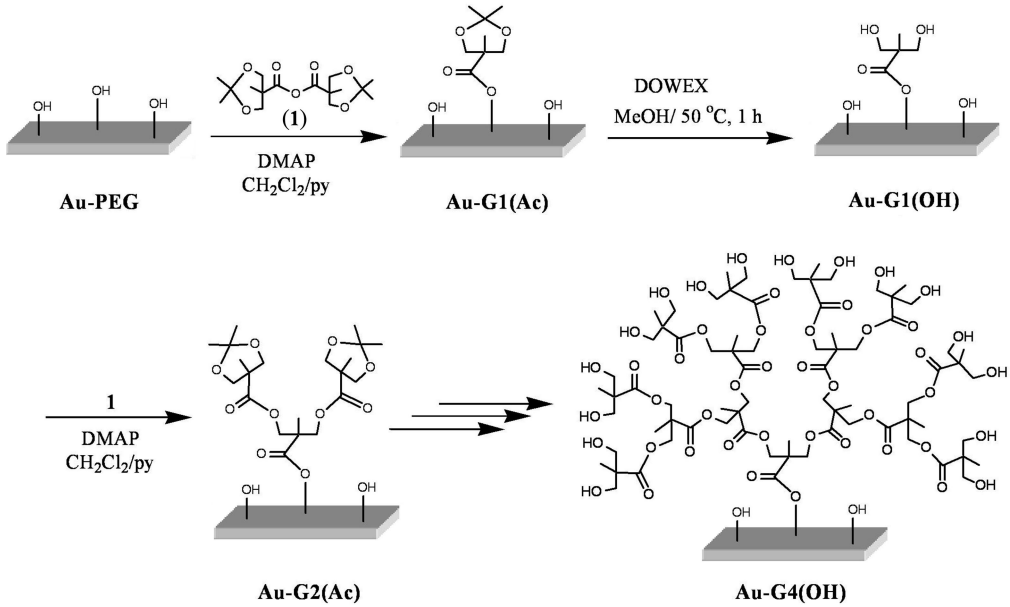

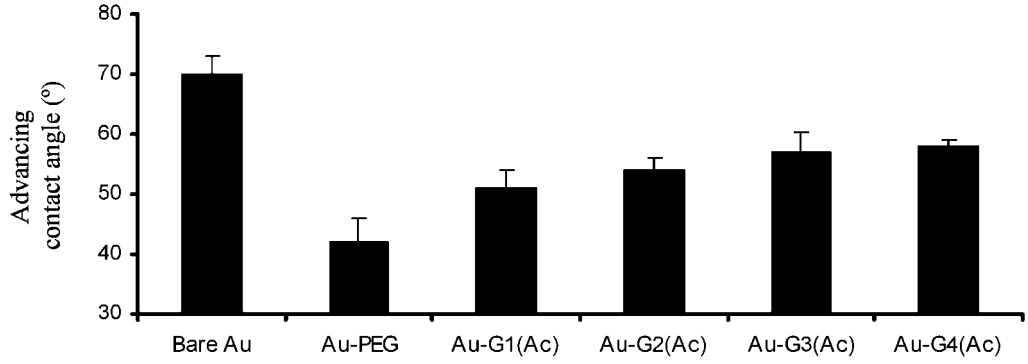

Figure 1. Advancing contact angles of Au, Au-PEG, and Au-G1(Ac) to G4(Ac) surfaces.

Table 2. Water Contact Angles of Unmodified Au, Au-PEG, and Au-G1(Ac) to G4(Ac)

surface	advancing contact angle (deg)	receding contact angle (deg)
bare Au	70 ± 3	40 ± 8
Au-PEG_{650}[a]	42 ± 4	36 ± 2
Au-G1(Ac)	51 ± 3	26 ± 5
Au-G2(Ac)	54 ± 2	31 ± 2
Au-G3(Ac)	57 ± 4	24 ± 2
Au-G4(Ac)	58 ± 1	33 ± 3

[a] 5 mM chemisorption solution of HS-PEG_{650}-OH in PBS at pH = 7.4 and high IS for 4 h.

Table 3. Water Contact Angles of Unmodified Au, Au-PEG, and Au-G1(OH) to G4(OH)

surface[a]	advancing contact angle (deg)	receding contact angle (deg)
bare Au	70 ± 3	40 ± 8
Au-PEG_{650}	42 ± 4	36 ± 2
Au-G1(OH)	40 ± 2	22 ± 3
Au-G2(OH)	36 ± 2	15 ± 1
Au-G3(OH)	32 ± 1	10 ± 1
Au-G4(OH)	30 ± 2	13 ± 1

[a] 5 mM chemisorption solution of HS-PEG_{650}-OH in PBS at pH = 7.4 and high IS for 4 h.

Water contact angles were also utilized to characterize the surfaces after each esterification and deprotection step of the divergent growth of dendrons at every generation. The results, summarized in Table 2 and Figure 1, show that the advancing contact angles for the protected dendritic generations ranged between 51 ± 3° and 58 ± 1°, and the receding angles ranged between 26 ± 5° and 33 ± 3° for generations 1−4. These increasing contact angle values reflect the hydrophobic character of the dendrons bearing the acetonide groups at their periphery (Table 2, Figure 1).

In contrast, the contact angles obtained after deprotection of the acetonide groups show a significant decrease when compared to the PEG-functionalized gold surfaces (Table 3, Figure 2). The advancing contact angles for the OH-terminated dendritic generations 1−4 ranged between 40 ± 2° and 30 ± 2°, and the receding angles ranged between 22 ± 3° and 13 ± 1°. These results reflect the hydrophilic character of the OH-terminated dendron periphery after removal of the acetonide groups. This hydrophilic character increases with increasing dendron generation as a result of the theoretical doubling in number of hydroxyl groups at the periphery from one generation to the next.

X-ray Photoelectron Spectroscopy (XPS). High-resolution XPS data for sulfur and carbon within each of the samples are summarized in Figure 3. The S 2p photoelectron peak at ~162 eV was assigned to the gold-bound sulfur atoms (S−Au) obtained for both PEG-grafted and G4-dendronized surfaces (Figure 3b,c). The C 1s peak at 284.6 eV, observed on the bare gold surfaces (used as a control), was assigned to aliphatic carbon contamination on gold, which was also seen with the low-resolution data (not included). Such surface contamination with carbonaceous material is extremely common and difficult to avoid. Deconvolution of the C 1s peak of the PEG-modified surfaces revealed two distinct peaks shown in Figure 3e. The presence of the new major peak at 286 eV, assigned to the ether carbons within each repeat unit of PEG, clearly demonstrated the presence of PEG at the surface (Figure 3d). Similarly, analysis of the G4(Ac) dendronized surfaces revealed two major signals at 284.6 and 286 eV after deconvolution of the C 1s peak as well as minor peaks at 287 and 290 eV corresponding to higher oxidation state carbons (Figure 3f). The main difference between the PEG-functionalized surface and the G4(Ac)-dendronized surface was the reversal in the intensity of the deconvoluted C 1s peaks corresponding to the aliphatic and ether carbons. In the case of the Au-PEG surface, the ratio of ether to aliphatic carbons is greater than 1, whereas in the case of Au-G4(Ac) surface, this ratio is less than 1 due to the larger number of aliphatic carbons resulting from multiple acetonide groups at the dendron periphery (data for Au-G1(Ac)

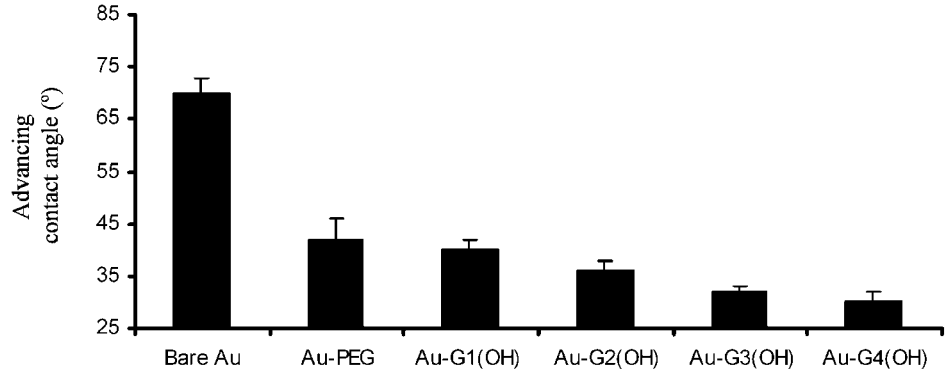

Figure 2. Advancing contact angles of Au, Au-PEG, and Au-G1(OH) to G4(OH) surfaces.

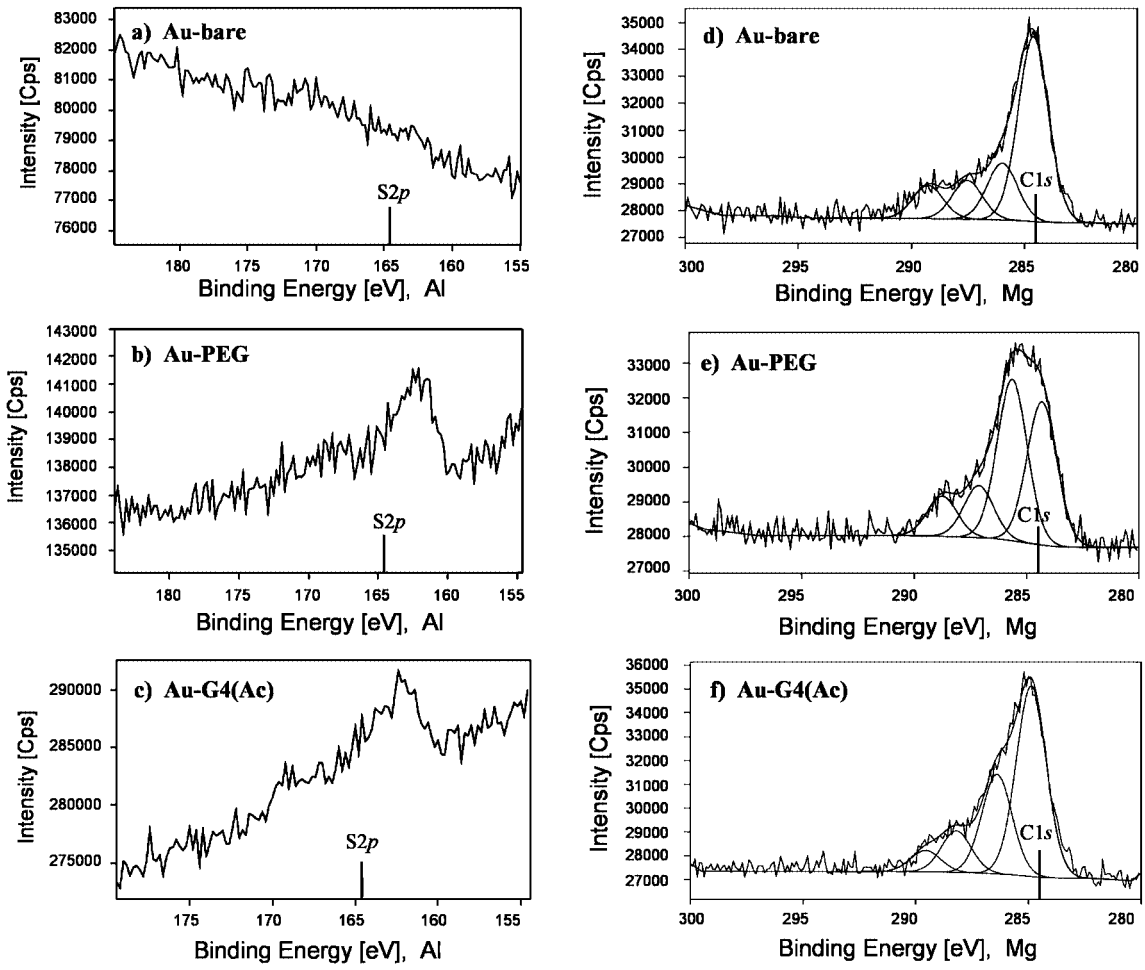

Figure 3. High-resolution S 2p XPS data at 90° takeoff angle for (a) bare Au, (b) Au-PEG, (c) Au-G1(Ac) and C 1s data at 90° takeoff angle for (d) bare Au, (e) Au-PEG, (f) Au-G4(Ac).

Table 4. Atomic Composition (%) Ratios from High-Resolution C 1s XPS Data for Various Surfaces

		(284.6:286 eV) C^a:*C*−O		(284.6:290 eV) C^a:*C*OO		(284.6:287 eV) C^a:*C*H_2OCO	
surface	takeoff angle (deg)	calcd	found	calcd	found	calcd	found
Au	90	0	3.26	0	5.56	0	4.8
	20	0	3.47	0	8.09	0	6.45
Au-PEG	90	0	0.88	0	3.54	0	2.75
	20	0	0.67	0	2.78	0	1.56
Au-G1(Ac)	90	0.18	2.5	5	6.88	2.5	5.44
	20	0.18	2.47	5	5.47	2.5	4.91
Au-G2(Ac)	90	0.36	1.92	3.33	4.57	1.67	4.49
	20	0.36	2.06	3.33	3.37	1.67	3.37
Au-G3(Ac)	90	0.71	1.68	2.86	3.66	1.43	3.57
	20	0.71	1.06	2.86	4.01	1.43	2.92
Au-G4(Ac)	90	1.42	1.67	2.67	2.19	1.33	2.66
	20	1.42	1.39	2.67	2.12	1.33	1.88

[a] Alipahtic carbons of the acetonide protecting groups within the dendrons.

to Au-G3(Ac) are given in the Supporting Information). Furthermore, for a more quantitative evaluation of surface functionalization, the ratios of the deconvoluted peaks obtained from the high-resolution C 1s analysis for each carbon environment were calculated and compared to the expected theoretical values (Table 4). The ratios were calculated for four specific carbon environments at binding energies of 284.6, 286, 287, and 290 eV, corresponding to aliphatic bis-MPA carbons, ether carbons (*C*−O−), ester carbons (−*C*H_2OCO−), and carbonyl carbons (−CH_2O*C*O−), respectively. These four carbon environments were specifically chosen to provide a direct comparison between the PEG carbons and the dendron carbons. All ratios were calculated in reference to the aliphatic bis-MPA C atoms. For instance, the ratio of the aliphatic carbons, present only in the dendrons, to the ether carbons, present only in the PEG chains, would be expected to increase as the dendron generation increases. The XPS data show that, as dendron generation increases, the agreement between measured and theoretically calculated ratios generally improves (Table 4).

Time-of-Flight Secondary Ion Mass Spectroscopy (TOF-SIMS). In order to further characterize the surface functionalization, all the surfaces were analyzed in detail using TOF-SIMS in both positive and negative modes. The major advantage of TOF-SIMS over XPS measurements is the ability to analyze only the outermost surface layer (∼5 Å) of a sample and provide not only information on the elemental composition of the surface but also the chemical structure of species on the surface. The

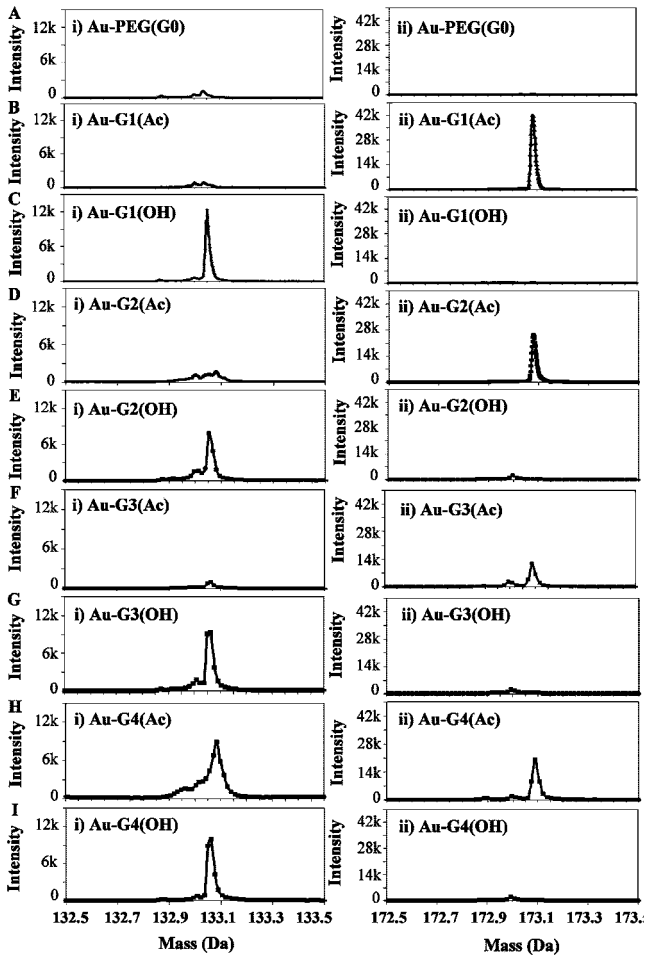

Figure 4. Normalized negative ion TOF-SIMS spectra of various surfaces for two mass ranges: (i) mass range corresponding to the deprotected G1(OH) fragment ($C_5H_9O_4$); (ii) mass range corresponding to the acetonide-protected fragment ($C_8H_{13}O_4$).

positive ion TOF-SIMS spectra of the bare Au, Au-G1(Ac), Au-G1(OH), and Au-G2(Ac) are shown in Figure 4 for two different mass ranges corresponding to two fragments specific to the immobilized dendrons. These two fragments, with molecular formula of $C_5H_9O_4^+$ (MW = 133.12 Da) and $C_8H_{13}O_4^+$ (MW = 173.19 Da), correspond to the deprotected and acetonide-protected bis-MPA units, respectively. Therefore, analyzing the TOF-SIMS spectra at these specific mass values for the various surfaces provided direct evidence of functionalization with the aliphatic polyester dendrons. (The full TOF-SIMS spectra over the entire mass range are provided in the Supporting Information.) For each surface, the observed molecular fragments corresponded to the species expected at the dendron periphery. For example, after reaction of the surfaces with the anhydride (**1**) at any dendron growth step, the TOF-SIMS spectra indicate the presence of the expected acetonide-protected fragment at 173 Da (Figure 4B(ii), D(ii), F(ii), and H(ii)). After any deprotection step, the spectra indicate the presence of a fragment at 133 Da, corresponding to the expected diol fragment (Figure 4C(i), E(i), G(i), and I(i)). Importantly, for the first three generations, the observed signals are mutually exclusive (i.e., the fragment at 133 Da is not observed in the samples measured after reaction with **1**, and the fragment at 173 is not observed after deprotection steps). Low-intensity signals observed in several samples were identified as fragments

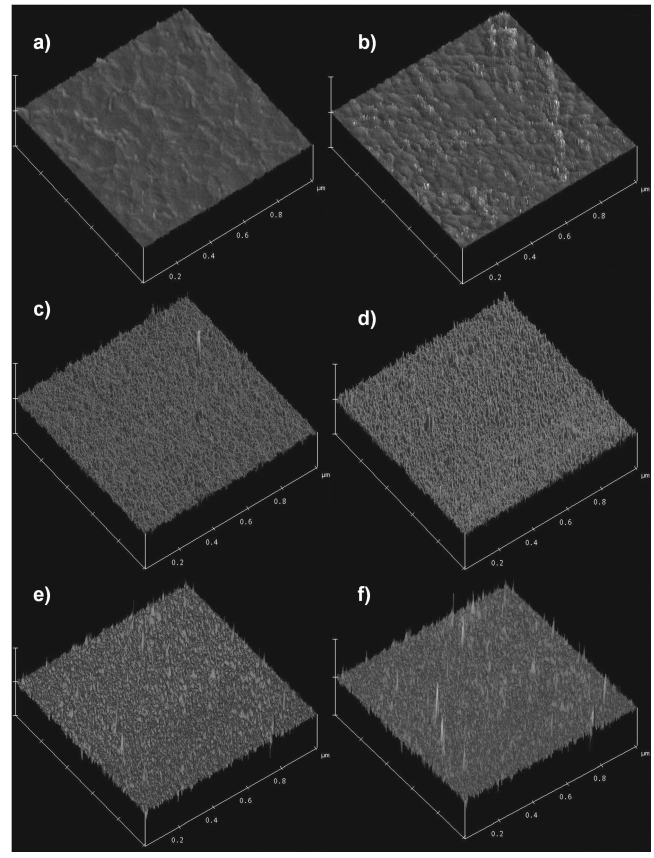

Figure 6. AFM amplitude images of (a) bare Au, (b) Au-PEG, (c) Au-G1(Ac), (d) Au-G2(Ac), (e) Au-G3(Ac), and (f) Au-G4(Ac) (image size: 1 × 1 μm^2).

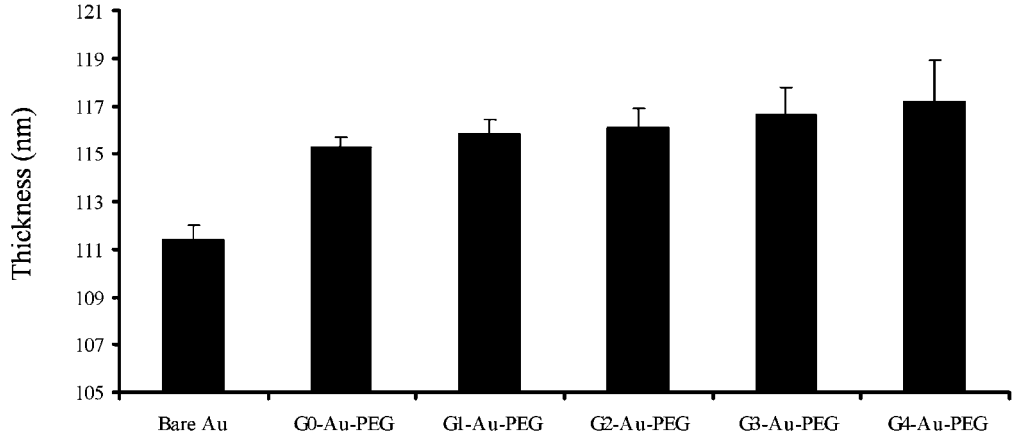

Figure 5. Film thickness measurement using Tapping Mode AFM height analysis.

Table 5. Root-Mean-Square (rms) Roughness of Bare and Modified Gold Surfaces Obtained from AFM Data

surface	rms (nm)
bare gold	1.26
Au-PEG_{650}	2.27
Au-G1(Ac)	2.41
Au-G2(Ac)	3.57
Au-G3(Ac)	4.04
Au-G4(Ac)	5.42

of PEG chains and small amounts of unreacted lower generation dendrons. From the data for higher generations, it is clear that dendron growth from G3 to G4 on the surfaces does not go to completion, as a significant signal is observed for the deprotected fragments (133 Da) at this stage. This decreased efficiency of the coupling step at higher generations is likely a result of increasing steric hindrance arising from the presence of bulky dendrons on the surface. Nevertheless, along with the XPS and contact angle results, these data illustrate that dendronization of the PEG-functionalized surfaces and subsequent divergent dendron growth using the iterative deprotection and coupling protocol (Scheme 1) were carried out successfully.

AFM Analysis. Ex-situ ellipsometry is the most widely used technique for film thickness measurement on smooth surfaces. However, the rough nature of gold surfaces (1–2 nm surface roughness) and the relatively small adsorbate thicknesses limited its use in the present work. Therefore, film thickness measurements of the chemisorbed PEG layer on gold were accomplished by Tapping Mode AFM height measurements using the "scratch" method. The average thickness of the gold layer measured on a clean surface prior to functionalization was found to be ~111.4 ± 0.6 nm, which is in good agreement with the expected thickness of 100 nm, as reported by the manufacturer. This result indicated that the scratch introduced onto the surface prior to functionalization penetrated the entire gold layer. This was important, since any gold remnants within the scratch could be grafted with PEG chains in the chemisorption step, resulting in inaccurate film thickness measurements. The film thickness data of the PEG-grafted surfaces (Au-PEG) show that the average thickness, measured at numerous points using the average mode calculation in the AFM Nanoscope-(R) III software, was ~115.3 ± 0.4 nm (see Supporting Information, Figure S2). Therefore, the thickness of the PEG chain layer was 3.9 ± 1 nm, which is in close agreement with the theoretical value of 4.1 nm calculated for the film thickness of a PEG_{650} layer based on the characteristic monomer length of 2.78 Å for the ethylene oxide repeat unit.[55]

The AFM thickness data obtained for the G1(Ac)−G4(Ac) dendronized surfaces show very little difference compared to the PEG layer thickness (Figure 5). These results were not surprising since the theoretical height of the grafted dendrons is expected to be less than 1 nm, which is within the error of the AFM measurements.

The surface topographies of the scratched gold surface prior to and after functionalization were also examined by AFM. The results from the 3D AFM amplitude images illustrated in Figure 6 show that the control gold surface prior to functionalization was relatively smooth, with a mean roughness (Ra) value of 1.26 nm (Figure 6a). In contrast, the surface roughness of the PEG-grafted surface increased to 2.27 nm (Figure 6b). The surface roughness increased considerably upon dendronization, with values ranging between 2.41 and 5.42 nm for the G1 to G4 dendronized surfaces (Figure 6c−f, Table 5).

The increase in surface roughness upon PEG functionalization is believed to be a result of PEG aggregation into phase-separated domains on the surface. Similar AFM results on PEG-modified surfaces were reported previously.[56,57] The continued increase in surface roughness upon dendronization is likely caused by additional local aggregation of hydrophobic acetonide-protected dendrons as their size increases. Furthermore, the general dendron shape and the incomplete surface dendronization at higher generations can both lead to increased surface roughness and heterogeneity.

Fibrinogen Adsorption. The effect of surface modification with PEG and its subsequent dendronization on protein adsorption was investigated. Fibrinogen (Fg) was selected for these studies due to the crucial role it plays in wound healing,[58] clot formation,[59] and platelet adhesion/activation.[56] Adsorption onto various surfaces was studied from both PBS−NaI buffer and plasma. Prior to adsorption, the protein was radiolabeled with ^{125}I, which enabled quantitative estimation of the amount of protein adsorbed onto the surfaces in units of $\mu g/cm^2$. This study was based on the previously reported results showing significant protein adsorption resistance of surfaces functionalized with PEG chains of various molecular weights.[3,12] Although the mechanism of protein repulsion in the presence of PEG is not fully understood, this effect was attributed to several factors, including chain density, length, flexibility, and PEG hydration due to its hydrophilic nature.[14,15,20,33,59] In the present work, we set out to determine whether or not the increased hydrophilicity introduced by dendron grafting could improve protein repulsion.

The results from the Fg adsorption studies show that the dendronized surfaces exhibit an opposite effect on protein adsorption to the one originally expected. The results obtained show that protein adsorption increased upon introducing the G1(OH) dendrons compared to the PEG-modified surfaces. Furthermore, protein adsorption continued to increase with increasing dendron generation as shown in Figure 7, despite the increase in surface hydrophilicity imparted by the dendrons. It has been proposed that one of the contributing factors to protein resistance on PEG-modified surfaces is PEG chain flexibility and dynamics, where it is believed that higher chain flexibility enhances protein repulsion.[3,12] In our studies, the increase in protein adsorption as a result of surface dendronization can potentially be explained by this hypothesis, as a decrease in PEG chain mobility can result from intra- and intermolecular hydrogen bonding of the grafted dendrons. The fact that protein adsorption increases with increasing dendron generation is consistent with this hypothesis, as higher dendron generations exhibit a greater number of peripheral OH groups, increasing the extent of inter- and intramolecular "locking" interactions.

Fibrinogen adsorption from plasma was also studied with 2.5% radio-iodinated fibrinogen following the same procedure used with PBS−NaI buffer. The results from these experiments show that the trend of adsorption from plasma is similar to the one observed from PBS−NaI solution (Table 6, Figure 8). Once again, the data show that PEG-modified surfaces significantly enhance fibrinogen repulsion with about 75% reduction compared to the control gold surfaces. However, functionalization of the PEG chains with the aliphatic polyester dendrons increases protein adsorption (Table 6, Figure 8).

Lysozyme Adsorption. Lysozyme was also selected for these studies in order to investigate the effect of protein size on adsorption to dendronized surfaces. Lysozyme is a relatively small protein (14.6 kDa) compared to fibrinogen (340 kDa), and therefore its adsorption onto the modified surfaces could be facilitated by easier diffusion through the dendronized PEG film. The results obtained from protein adsorption from PBS−NaI buffer show that the trend of protein resistance to lysozyme is similar to the one observed with fibrinogen (Figure 9). On the basis of this data, it is clear that the molar quantity of lysozyme deposited on the various surfaces is much higher than that of fibrinogen, as expected due to the difference in protein size.

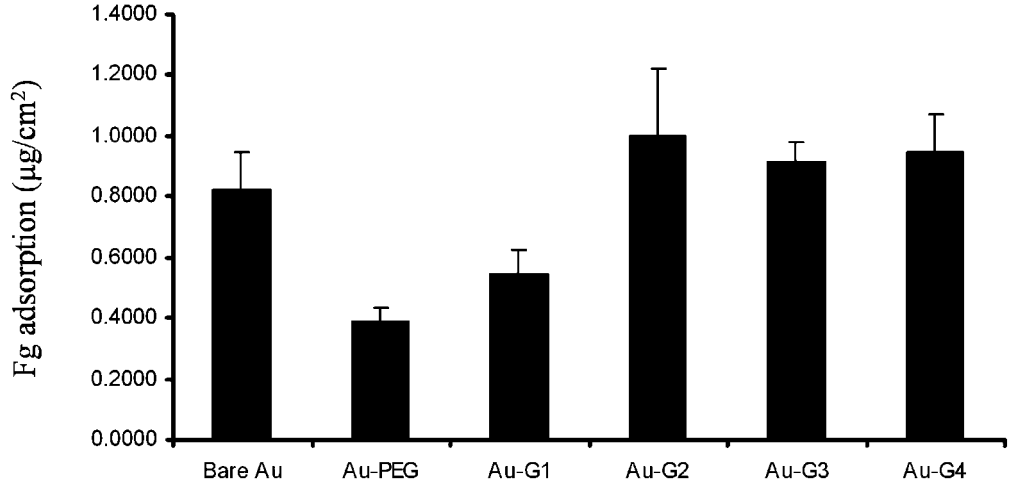

Figure 7. Fibrinogen adsorption from PBS buffer: effect of surface modification with PEG and dendronization with aliphatic polyester dendrons G1−G4.

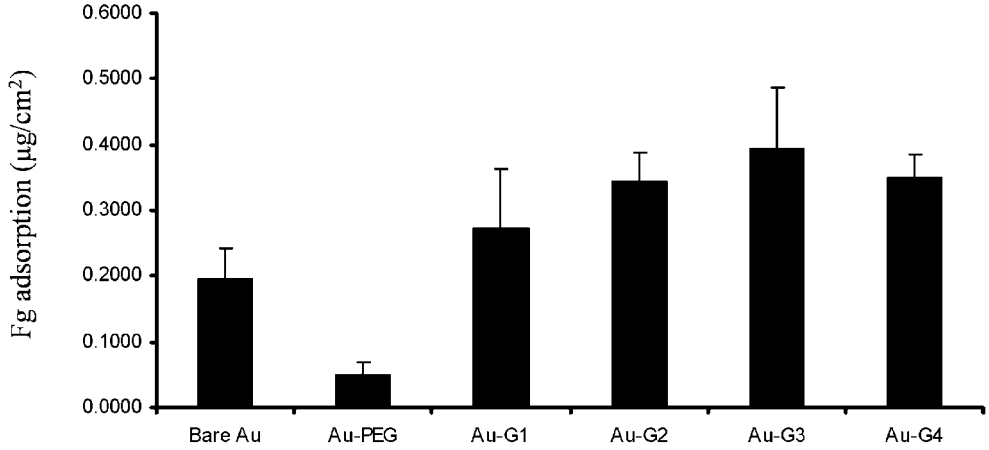

Figure 8. Fibrinogen adsorption from plasma: effect of surface modification with PEG and dendronization with aliphatic polyester dendrons G1−G4.

The molar ratios of adsorbed Ly:Fg are given in Table 7 and range from 12.8 to 29.2.

Conclusions

Modification of gold-coated silicon wafers with monothiolated PEG_{650} was carried out using high ionic strength (IS = 2.9 M) chemisorption solutions for 4 h. Following chemisorption with PEG, the advancing water contact angles decreased significantly compared to the control gold surfaces, indicating an increase in hydrophilicity associated with the PEG chains. High-resolution C 1s XPS data indicated the presence of a new peak at 286 eV corresponding to ether linkages following chemisorption of the gold surfaces with HS-PEG_{650}-OH. High-resolution S 2p data showed a photoelectron peak at ~162 eV corresponding to the gold-bound sulfur atoms on the surfaces following PEG grafting, providing further evidence for the presence of PEG chains covalently attached to the surfaces. Further modification of the PEG-grafted surfaces was achieved via divergent dendron growth to introduce aliphatic polyester dendrons, generations 1−4, at the PEG-OH chain ends. Characterization of the G1−G4 dendronized surfaces using water contact angles showed a decrease in contact angle with increasing dendron generation for the deprotected OH-terminated dendrons, indicating an increase in hydrophilicity imparted by the gradually increasing number of peripheral OH groups. The TOF-SIMS results provided detailed structural information of the functionality on the surface. Looking at the signals corresponding to specific peaks belonging to the dendron structure, the transition from the PEG-grafted surfaces to the dendronized ones was clearly demonstrated. In agreement with previously reported protein adsorption studies, PEG-modified surfaces exhibited a decrease in protein adsorption compared to the control gold surfaces. However, it was found that protein adsorption increased upon dendronization of the PEG-modified surfaces, suggesting that PEG chain flexibility may be one of the key factors in the mechanism of protein resistance. This chain flexibility is impeded by introducing dendrons with multiple peripheral OH groups, which can lock the PEG chains via inter- and/or intramolecular H-bonding. Future studies will focus on functionalization of the peripheral OH groups of dendronized surfaces with PEG chains in order to increase surface coverage with PEG and retrieve chain flexibility.

Acknowledgment. Financial support for this work was provided by the Natural Science and Engineering Council of Canada (NSERC), the Canadian Institutes for Health Research (CIHR), the Canada Foundation for Innovation (CFI), and the Ontario Innovation Trust (OIT). Dr. Rana Sodhi for his help with the XPS analyses and curve fitting assistance and Peter Brodersen for his help with the TOF-SIMS analysis.

Supporting Information Available: High-resolution XPS data, AFM monolayer height analysis, and full TOF-SIMS spectra. This material is available free of charge via the Internet at http://pubs.acs.org.

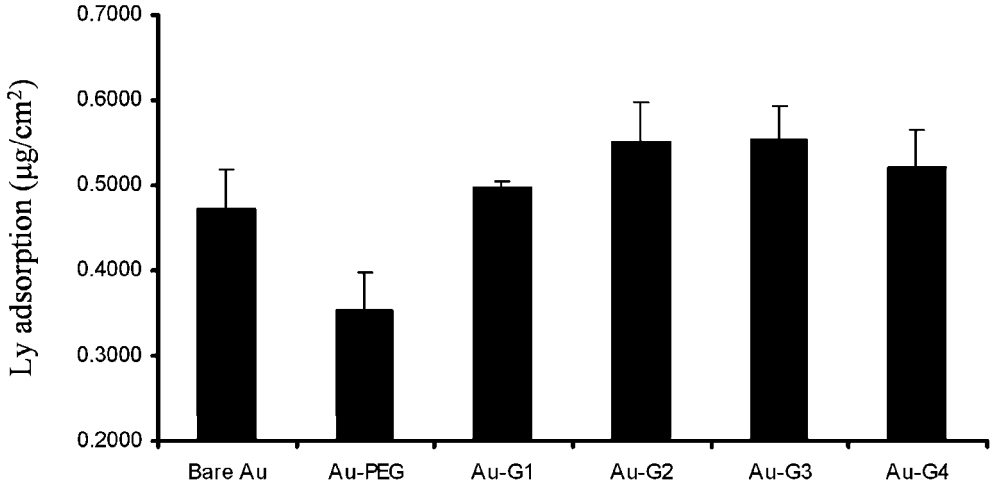

Figure 9. Lysozyme adsorption from PBS buffer: effect of surface modification with PEG and dendronization with aliphatic polyester dendrons G1−G4.

Table 6. Fibrinogen Reduction from PBS−NaI and Plasma of Various Surfaces

surface	Fg PBS−NaI (μg/cm^2)	reduction vs control (%)[a]	Fg plasma (μg/cm^2)	reduction vs control (%)[a]
bare Au	0.82 ± 0.12		0.20 ± 0.05	
Au-PEG$_{650}$	0.28 ± 0.05	66	0.05 ± 0.02	75
Au-G1(OH)	0.54 ± 0.08	34	0.32 ± 0.09	-60^b
Au-G2(OH)	1.00 ± 0.20	-22^b	0.51 ± 0.03	-155^b
Au-G3(OH)	0.91 ± 0.06	-11^b	0.54 ± 0.15	-170^b
Au-G4(OH)	0.94 ± 0.14	-15^b	0.42 ± 0.01	-110^b

[a] The value for bare Au was used as the control. [b] Negative values indicate a higher protein adsorption relative to bare Au.

Table 7. Comparison between Fibrinogen and Lysozyme Adsorption

surface	fibrinogen (μg/cm^2)	reduction vs control (%)[a]	lysozyme (μg/cm^2)	reduction vs control (%)[a]	molar ratio Ly:Fg
bare Au	0.82 ± 0.1		0.47 ± 0.05		13.4
Au-PEG$_{650}$	0.28 ± 0.05	66	0.35 ± 0.04	26	29.2
Au-G1(OH)	0.54 ± 0.08	34	0.50 ± 0.01	-6^b	21.5
Au-G2(OH)	1.00 ± 0.2	-22^b	0.55 ± 0.05	-17^b	12.8
Au-G3(OH)	0.91 ± 0.06	-11^b	0.55 ± 0.04	-17^b	14.1
Au-G4(OH)	0.94 ± 0.14	-15^b	0.52 ± 0.04	-11^b	12.9

[a] The value for bare Au was used as the control. [b] Negative values indicate a higher protein adsorption relative to bare Au.

References and Notes

(1) Castner, D. G.; Ratner, B. D. *Surf. Sci.* **2002**, *500*, 28–60.
(2) Kane, R. S.; Deschatelets, P.; Whitesides, G. M. *Langmuir* **2003**, *19*, 2388–2391.
(3) Unsworth, L. D.; Sheardown, H.; Brash, J. L. *Langmuir* **2005**, *21*, 1036–1041.
(4) Santini, J. T.; Cima, M. J.; Langer, R. *Nature (London)* **1999**, *397*, 335–338.
(5) Xu, F. J.; Li, Y. L.; Kang, E. T.; Neoh, K. G. *Biomacromolecules* **2005**, *6*, 1759–1768.
(6) Frazier, R. A.; Matthijs, G.; Davies, M. C.; Roberts, C. J.; Schacht, E.; Tendler, S. J. B. *Biomaterials* **2000**, *21*, 957–966.
(7) Rabinow, B. E.; Ding, Y. S.; Qin, C.; Mchalsky, M. L.; Schneider, J. H.; Ashline, K. A.; Shelbourn, T. L.; Albrecht, R. M. *J. Biomater. Sci., Polym. Ed.* **1994**, *6*, 91–109.
(8) Lehmann, T.; Ruhe, J. *Macromol. Symp.* **1999**, *142*, 1–12.
(9) Heyes, C. D.; Groll, J.; Moeller, M.; Nienhaus, G. U. *Mol. Biosyst.* **2007**, *3*, 419–430.
(10) Sofia, S. J.; Premnath, V.; Merrill, E. W. *Macromolecules* **1998**, *31*, 5059–5070.
(11) Yang, Z. H.; Galloway, J. A.; Yu, H. U. *Langmuir* **1999**, *15*, 8405–8411.
(12) Unsworth, L. D.; Sheardown, H.; Brash, J. L. *Biomaterials* **2005**, *26*, 5927–5933.
(13) Zolk, M.; Eisert, F.; Pipper, J.; Herrwerth, S.; Eck, W.; Buck, M.; Grunze, M. *Langmuir* **2000**, *16*, 5849–5852.
(14) Jeon, S. I.; Andrade, J. D. *J. Colloid Interface Sci.* **1991**, *142*, 159–166.
(15) Jeon, S. I.; Lee, J. H.; Andrade, J. D.; de Gennes, P. G. *J. Colloid Interface Sci.* **1991**, *142*, 149–158.
(16) Albertsson, A. C.; Karlsson, S. *J. Macromol. Sci., Pure Appl. Chem.* **1996**, *A33*, 1565–1570.
(17) Wang, R. L. C.; Kreuzer, H. J.; Grunze, M. *J. Phys. Chem. B* **1997**, *101*, 9767–9773.
(18) Morra, M. *J. Biomater. Sci., Polym. Ed.* **2000**, *11*, 547–569.
(19) Nagaoka, S.; Mori, Y.; Takiuchi, H.; Yokota, K.; Tanzawa, H.; Nishiumi, S. In *Polymers as Biomaterials*; Shalaby, S. W., Hoffman, A. S., Ratner, B. D., Horbett, T. A., Eds.; Plenum: New York, 1984; pp 661–374.
(20) Andrade, J. D.; Hlady, V. *Adv. Polym. Sci.* **1986**, *79*, 1–63.
(21) Harder, P.; Grunze, M.; Dahint, R.; Whitesides, G. M.; Laibinis, P. E. *J. Phys. Chem. B* **1998**, *102*, 426–436.
(22) Unsworth, L. D.; Tun, Z.; Sheardown, H.; Brash, J. L. *J. Colloid Interface Sci.* **2006**, *296*, 520–526.
(23) Wojciechowski, P.; Tenhove, P.; Brash, J. L. *J. Colloid Interface Sci.* **1986**, *111*, 455–465.
(24) Ostmark, E.; Macakova, L.; Auletta, T.; Malkoch, M.; Malmstrom, E.; Blomberg, E. *Langmuir* **2005**, *21*, 4512–4519.
(25) Gillies, E. R.; Frechet, J. M. J. *J. Am. Chem. Soc.* **2002**, *124*, 14137–14146.
(26) Haag, R.; Sunder, A.; Stumbe, J. F. *J. Am. Chem. Soc.* **2000**, *122*, 2954–2955.
(27) Lee, C. C.; MacKay, J. A.; Frechet, J. M. J.; Szoka, F. C. *Nat. Biotechnol.* **2005**, *23*, 1517–1526.
(28) Yam, C. M.; Deluge, M.; Tang, D.; Kumar, A.; Cai, C. Z. *J. Colloid Interface Sci.* **2006**, *296*, 118–130.
(29) Sunder, A.; Mulhaupt, R.; Haag, R.; Frey, H. *Adv. Mater.* **2000**, *12*, 235–239.
(30) Siegers, C.; Biesalski, M.; Haag, R. *Chem.—Eur. J.* **2004**, *10*, 2831–2838.

(31) Hong, M. Y.; Yoon, H. C.; Kim, H. S. *Langmuir* **2003**, *19*, 4866–4866.
(32) Hong, M. Y.; Kim, Y. J.; Lee, J. W.; Kim, K.; Lee, J. H.; Yoo, J. S.; Bae, S. H.; Choi, B. S.; Kim, H. S. *J. Colloid Interface Sci.* **2004**, *274*, 41–48.
(33) Ostuni, E.; Chapman, R. G.; Holmlin, R. E.; Takayama, S.; Whitesides, G. M. *Langmuir* **2001**, *17*, 5605–5620.
(34) Ihre, H. R.; De Jesus, O. L. P.; Szoka, F. C.; Frechet, J. M. J. *Bioconjugate Chem.* **2002**, *13*, 443–452.
(35) De Jesus, O. L. P.; Ihre, H. R.; Gagne, L.; Frechet, J. M. J.; Szoka, F. C. *Bioconjugate Chem.* **2002**, *13*, 453–461.
(36) Malkoch, M.; Malmstrom, E.; Hult, A. *Macromolecules* **2002**, *35*, 8307–8314.
(37) Du, Y. J.; Cornelius, R. M.; Brash, J. L. *Colloids Surf., B* **2000**, *17*, 59–67.
(38) Kingshott, P.; Thissen, H.; Griesser, H. J. *Biomaterials* **2002**, *23*, 2043–2056.
(39) Ihre, H.; De Jesus, O. L. P.; Frechet, J. M. J. *J. Am. Chem. Soc.* **2001**, *123*, 5908–5917.
(40) Vestberg, R.; Nystrom, A.; Lindgren, M.; Malmstrom, E.; Hult, A. *Chem. Mater.* **2004**, *16*, 2794–2804.
(41) Wu, P.; Malkoch, M.; Hunt, J. N.; Vestberg, R.; Kaltgrad, E.; Finn, M. G.; Fokin, V. V.; Sharpless, K. B.; Hawker, C. J. *Chem. Commun.* **2005**, 5775–5777.
(42) Vestberg, R.; Westlund, R.; Eriksson, A.; Lopes, C.; Carlsson, M.; Eliasson, B.; Glimsdal, E.; Lindgren, M.; Malmstrom, E. *Macromolecules* **2006**, *39*, 2238–2246.
(43) Yim, S. H.; Huh, J.; Ahn, C. H.; Park, T. G. *Macromolecules* **2007**, *40*, 205–210.
(44) Goh, S. L.; Francis, M. B.; Frechet, J. M. J. *Chem. Commun.* **2002**, 2954–2955.
(45) Liang, C. O.; Helms, B.; Hawker, C. J.; Frechet, J. M. J. *Chem. Commun.* **2003**, 2524–2525.
(46) Malkoch, M.; Carlmark, A.; Wodegiorgis, A.; Hult, A.; Malmstrom, E. E. *Macromolecules* **2004**, *37*, 322–329.
(47) Malkoch, M.; Thibault, R. J.; Drockenmuller, E.; Messerschmidt, M.; Voit, B.; Russell, T. P.; Hawker, C. J. *J. Am. Chem. Soc.* **2005**, *127*, 14942–14949.
(48) Lee, C. C.; Frechet, J. M. J. *Macromolecules* **2006**, *39*, 476–481.
(49) Hietala, S.; Nystrom, A.; Tenhu, H.; Hult, A. *J. Polym. Sci., Part A: Polym. Chem.* **2006**, *44*, 3674–3683.
(50) Nystrom, A.; Malkoch, M.; Furo, I.; Nystrom, D.; Unal, K.; Antoni, P.; Vamvounis, G.; Hawker, C.; Wooley, K.; Malmstrom, E.; Hult, A. *Macromolecules* **2006**, *39*, 7241–7249.
(51) Ihre, H.; Hult, A.; Frechet, J. M. J.; Gitsov, I. *Macromolecules* **1998**, *31*, 4061–4068.
(52) Ling, F. H.; Lu, V.; Svec, F.; Frechet, J. M. J. *J. Org. Chem.* **2002**, *67*, 1993–2002.
(53) Lonnberg, H.; Zhou, Q.; Brumer, H.; Teeri, T. T.; Malmstrom, E.; Hult, A. *Biomacromolecules* **2006**, *7*, 2178–2185.
(54) King, D. E. *J. Vac. Sci. Technol. A* **1995**, *13*, 1247–1253.
(55) Malmsten, M.; Emoto, K.; Van Alstine, J. M. *J. Colloid Interface Sci.* **1998**, *202*, 507.
(56) Chen, H.; Brook, M. A.; Sheardown, H. *Biomaterials* **2004**, *25*, 2273–2282.
(57) McGurk, S. L.; Green, R. J.; Sanders, G. H. W.; Davies, M. C.; Roberts, C. J.; Tendler, S. J. B.; Williams, P. M. *Langmuir* **1999**, *15*, 5136–5140.
(58) Unsworth, L. D.; Sheardown, H.; Brash, J. L. *Langmuir* **2005**, *21*, 1036–1041.
(59) Shen, M. C.; Horbett, T. A. *J. Biomed. Mater. Res.* **2001**, *57*, 336–345.

MA702074V